Supporting Information

for Macromol. Rapid Commun., DOI: 10.1002/marc.201800530

Carbohydrate-based Polymer Brushes Prevent Viral Adsorption on Electrostatically Heterogeneous Interfaces

Ramya Kumar,[†,⊥] Domenic Kratzer,[‡] Kenneth Cheng,[¶,⊥] Julia Prisby,[§,⊥] James Sugai,[‖] William V. Giannobile,[‖] and Joerg Lahann*[,†,¶,§,‡,⊥]

Supporting information

Carbohydrate-based Polymer Brushes Prevent Viral Adsorption on Electrostatically Heterogeneous Interfaces

Ramya Kumar,[†,⊥] Domenic Kratzer,[‡] Kenneth Cheng,[¶,⊥] Julia Prisby,[§,⊥] James Sugai,[‖] William V. Giannobile,[‖] and Joerg Lahann[*,†,¶,§,‡,⊥]

†*Department of Chemical Engineering, University of Michigan*

‡*Instituite of Functional Interfaces, Karlsruhe Institute of Technology*

¶*Department of Material Science & Engineering, University of Michigan*

§*Department of Biomedical Engineering, University of Michigan*

‖*School of Dentistry, University of Michigan*

⊥*Biointerfaces Institute, University of Michigan*

E-mail: lahann@umich.edu

1 Predictive models of virus-polymer interactions: Identifying key surface design variables

Before evaluating viral and protein adhesion, we wished to identify the surface design variables that would exert the most influence. First, we employed a statistical treatment developed by Duffadar et al.[1] to calculate the capture efficiency of viral particles by brush-free copolymer surfaces composed of AM and EB moieties. In this calculation, we assume that the AM groups are randomly distributed on the copolymer surface according to the Poisson distribution. Despite the existence of an overall or global negative zeta potential on the copolymer coatings, the AM groups provide "hotspots" of local positive charge to which viral particles can bind through point-wise interactions. However, these interactions cannot be predicted if we consider the averaged out surface charge of the copolymer coatings. Though DLVO theory predicts repulsive interactions between negatively charged particles and surfaces with a net negative ζ-potential, viral adsorption can still occur if the number of attractive elements present on the surface exceeds the threshold value.[2] A statistical treatment is capable of identifying this threshold, which is dependent on several variables-: ionic strength, contact area between the virus and the surface and the pH-dependent degree of ionization of the AM groups.

At a pH value of 4, (Figure S1a), the probability of capturing a viral particle with a radius of 20 nm increases monotonically as we add more AM groups to the surface, before hitting a plateau AM concentration where the likelihood of viral adsorption reaches 100%. Additionally, as the environment becomes less acidic (at a pH value of 5), the capture probabilities are greatly reduced even at the same copolymer composition (Figure S1b). This is because a lower proportion of AM groups are likely to be protonated at a pH of 5, rendering viral capture less probable. Viral radius emerged as another pertinent factor, with a particle radius of 20 nm resulting in lowered capture efficiencies (Figures S1c and S1d). We attribute this to the reduction in the contact area over which electrostatic forces

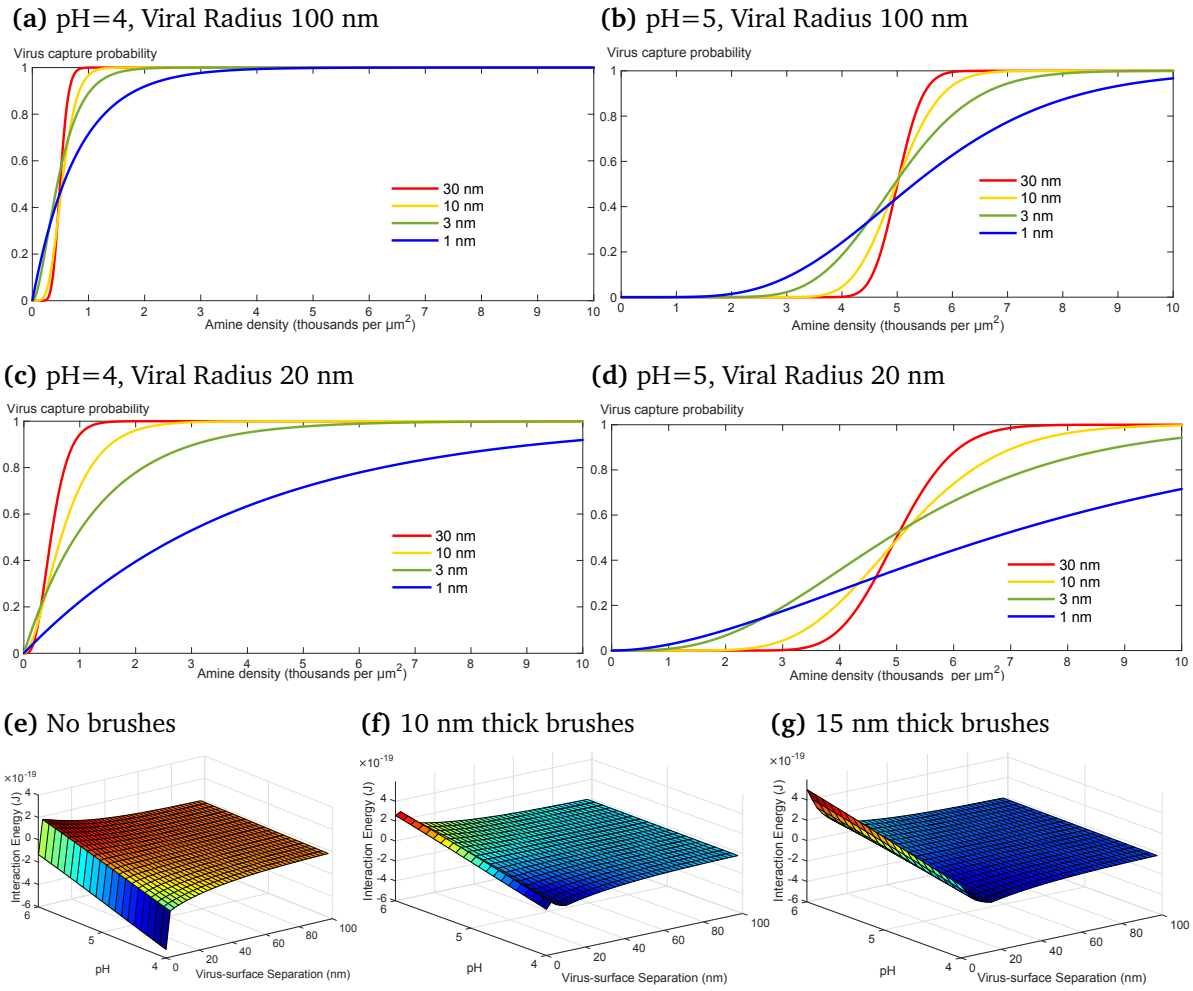

Figure S1. (a)-(d) Statistical models describe the probability of capturing viruses on copolymer surfaces (IEP of 4.9) when polymer brushes are absent. The probability is calculated as a function of copolymer compositions (amine density), pH values (4 or 5), Debye Lengths (red: 30 nm, yellow: 10 nm, green: 3 nm, blue: 1 nm) and viral radii (20 nm or 100 nm). (e) At pH values above the copolymer isoelectric point (4.9), repulsive interaction energy was calculated whereas attractive interactions were observed below the IEP. (f) When a 10 nm thick layer of polymer brushes is introduced, repulsive interactions gradually begin to dominate over a larger range of pH values. (g) When the brush thickness is increased further to 15 nm, repulsive interactions prevail over the entire pH range.

are exerted. Finally the dependence on capture efficiency on the density of AM electrostatic tethers can range from sigmoid at low ionic strength (Debye length of 30 nm) to linear at higher ionic strength (1 nm) (Figure S1d), underscoring the subtle but significant role played by ionic strength.

To conclude, when polymer brushes are absent, viral adhesion is largely shaped by extrinsic factors such as the ionic environment and the viral geometry, while intrinsic variables such as the surface composition play a smaller role. Since the magnitude and length scale of electrostatic repulsion exerted by the AM-containing copolymer surface are dependent on pH and Debye length respectively, the surface cannot be shielded from viruses merely by minimizing the AM density. Reduction of local electrostatic driving forces by controlling the AM density is therefore not a reliable strategy to control viral adhesion. This analysis underscores the necessity of a design element that functions as a barrier against adsorbing viral particles, namely polymer brushes with the optimal architecture and composition.

To investigate the effects of polymer brush thickness and density on the thermodynamics of virus-surface interactions, we performed DLVO calculations by employing a mean-field approximation.[2] For a copolymer surface with an isoelectric point (IEP) of 4.9 and a viral radius of 20 nm, we quantified the energy of the virus-surface interaction as a function of pH and the distance separating the virus from the copolymer surface. The electrostatic repulsion (or attraction) arising from the electrical double layer forces was added to the Van Der Waals attraction. In Figure S1e, we can see that when the pH is above the IEP of the copolymer, the virus is repelled from the surface whereas attractive interactions result at pH values lower than the IEP (4.9). However, when a 10 nm thick polymer brush is introduced (Figure S1f), the interaction energy assumes positive values, indicating that it becomes thermodynamically unfavorable for the virus to adhere to the surface across a broad range of pH values. When the brush thickness is increased further to 15 nm (Figure S1g), the height of the energy barrier forbidding viral adhesion only

grows further. Viruses adsorb to the surface in two modes -: either they penetrate the polymer brushes in regions where the brush character is compromised by the interspersed AM groups, or the virus compresses the brush, resulting in a decrease in brush height. In the latter case, the brush compression imposes an entropic penalty and carries high thermodynamic costs, whereas in the former case, excluded volume interactions prohibit viral penetration of the brush. Irrespective of the mechanism involved, we expect polymer brushes to prevent viral adsorption, possibly through phenomena that resemble those involved in protein resistance. In our model, we have only included the effects of entropic loss and steric repulsion. In reality, the water structure associated with the exceptionally hydrophilic glycopolymer brushes will also be disrupted by the adsorbed virus, giving rise to hydration repulsion caused by displacement of water molecules. However, hydration repulsion has not been accounted for in our model. Notwithstanding this approximation, our modeling study predicts that the thermodynamic landscape of virus-polymer interactions is transformed by the incorporation of the polymer brushes, with brush density and thickness emerging as key design variables.

2 XPS characterization

XPS analysis (Figure S2) of the mannose brushes revealed that the elemental composition was in close agreement with the theoretical values derived from the molecular structure. High resolution scans of the C_{1s} region (Figure S2d) were performed in order to quantify signals from the aliphatic C-C bonds, the C-C-O bonds from the pyranose ring, the N-C bonds and the C=O from the acrylamide. The distribution of areas under each of the fitted peaks matches the theoretical contribution from each component, which provides additional validation that the α-mannose brushes were present (Figure S2b). Overall, from our characterization studies, we were able to confirm that all four surfaces were successfully synthesized and that the chemical structure of α-mannose side chains remained intact after SI-ATRP. XPS measurements were also performed for glucose and galactose brushes

grafted from the reference polymer (Figures S3 and S4)

(a)

Binding energy eV	C 1s 285	N 1s 399	O 1s 532
Exp. (atom %)	66.6	5.0	28.3
Theo. (atom %)	57.8	5.2	36.8

(b)

Binding energy eV	C-C 285	C-C-O 286	N-C 287.6	C=O 288.8
Exp. (%)	25.4	55.7	17.3	1.7
Theo. (%)	38.9	44.4	11.1	5.6

(c)

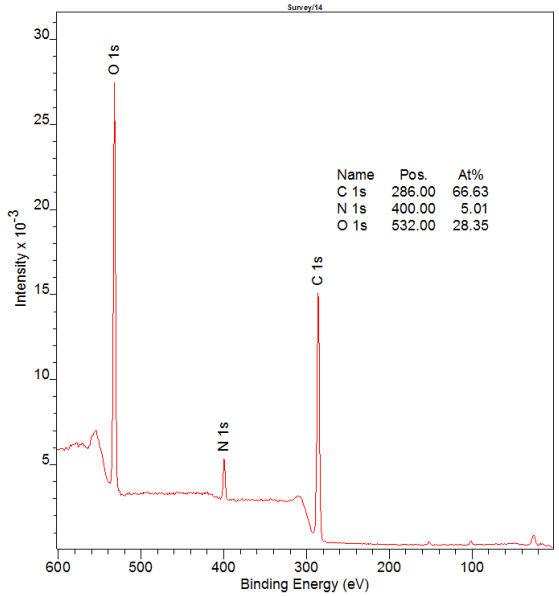

(d)

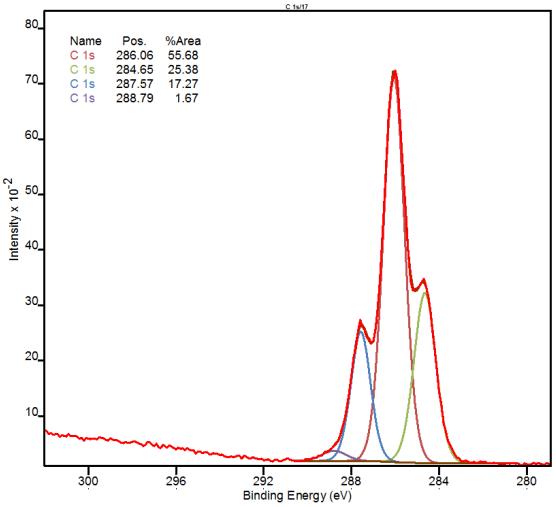

Figure S2. XPS characterization of poly(2'-acrylamidoethyl-α-d-mannopyranoside) brushes grafted from reference polymers. (A) Elemental composition of α-mannose brushes as measured using high resolution XPS scans. (B) & (D) High resolution XPS spectra of C_{1s} further confirms the chemical composition of the α-mannose brushes. (C) XPS Survey spectra of the surface bearing α-mannose brushes.

(a)

Binding energy eV	C 1s 285	N 1s 399	O 1s 532
Exp. (atom %)	61.5	5.1	33.3
Theo. (atom %)	57.8	5.2	36.8

(b)

Binding energy eV	C-C 285	C-C-O 286	N-C 287.6	C=O 288.8
Exp. (%)	20.0	56.5	17.8	5.6
Theo. (%)	38.9	44.4	11.1	5.6

(c)

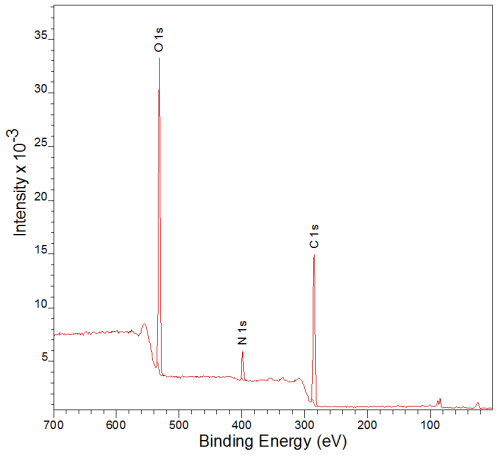

(d)

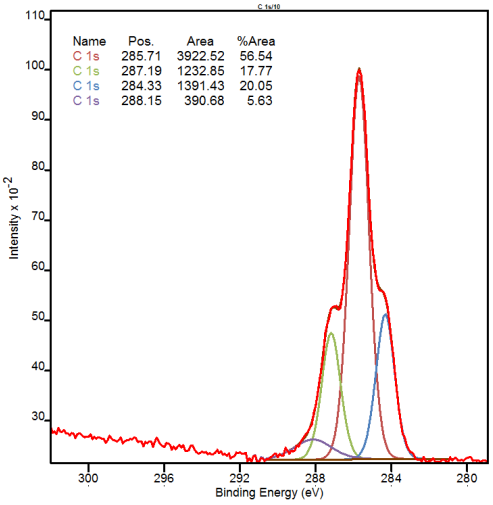

Figure S3. XPS characterization of poly(2'-acrylamidoethyl-β-d-glucopyranoside) brushes grafted from reference polymers. (a) Elemental composition of β-glucose brushes as measured using high resolution XPS scans. (b) & (d) High resolution XPS spectra of Carbon further confirms the chemical composition of the β-glucose brushes. (c) XPS survey spectra of the surface bearing β-glucose brushes.

(a)

Binding energy eV	C 1s 285	N 1s 399	O 1s 532
Exp. (atom %)	66.1	5.0	28.8
Theo. (atom %)	57.8	5.2	36.8

(b)

Binding energy eV	C-C 284.5	C-C-O 285.9	N-C 287.6	C=O 288.6
Exp.(%)	36.9	37.2	21.0	4.9
Theo. (%)	38.9	44.4	11.1	5.6

(c) **(d)**

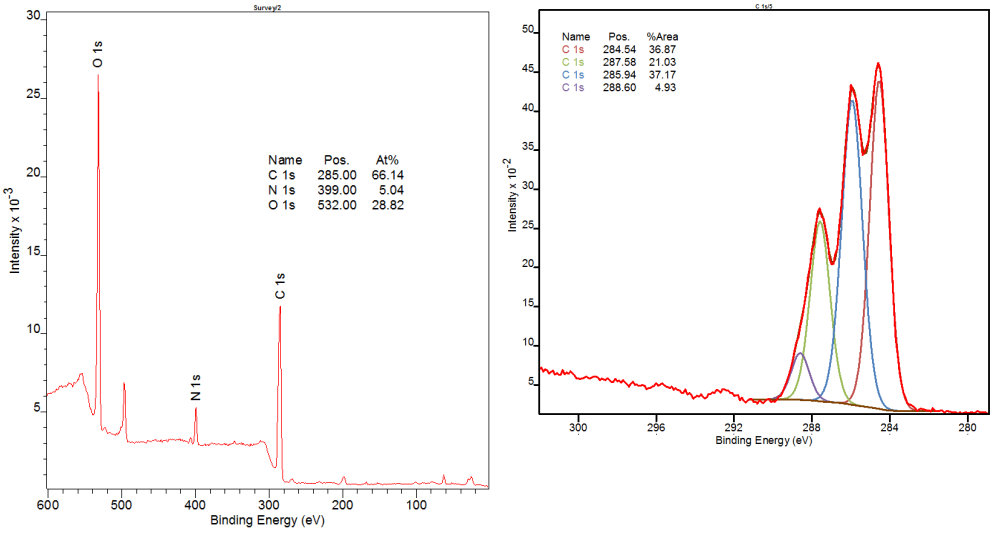

Figure S4. XPS characterization of poly(2'-acrylamidoethyl-β-d-galactopyranoside) brushes grafted from reference polymers. (a) Elemental composition of β-galactose brushes as measured using high resolution XPS scans. (b) & (d) High resolution XPS spectra of Carbon further confirms the chemical composition of the β-galactose brushes. (c) XPS survey spectra of the surface bearing β-galactose brushes.

3 Roughness measurements

To confirm that the differences in viral and protein adhesion were caused by the presence of AM groups and brush architecture alone and and not induced by roughness differences, we performed an AFM study of all the coatings used in our study. Differences in roughness between coatings were not significant (Figure S5). Three replicates were performed for each sample using a scan area of 0.5 $\times$ 0.5 micron, 0.977 Hz and an AFM tip of spring constant 40-75 N/m (Bruker ScanAsyst Air). Roughness values in the form of root mean square roughness (R_a) were acquired through a statistical analysis performed by the AFM software (NanoScope Analysis) by averaging over the scanned region.

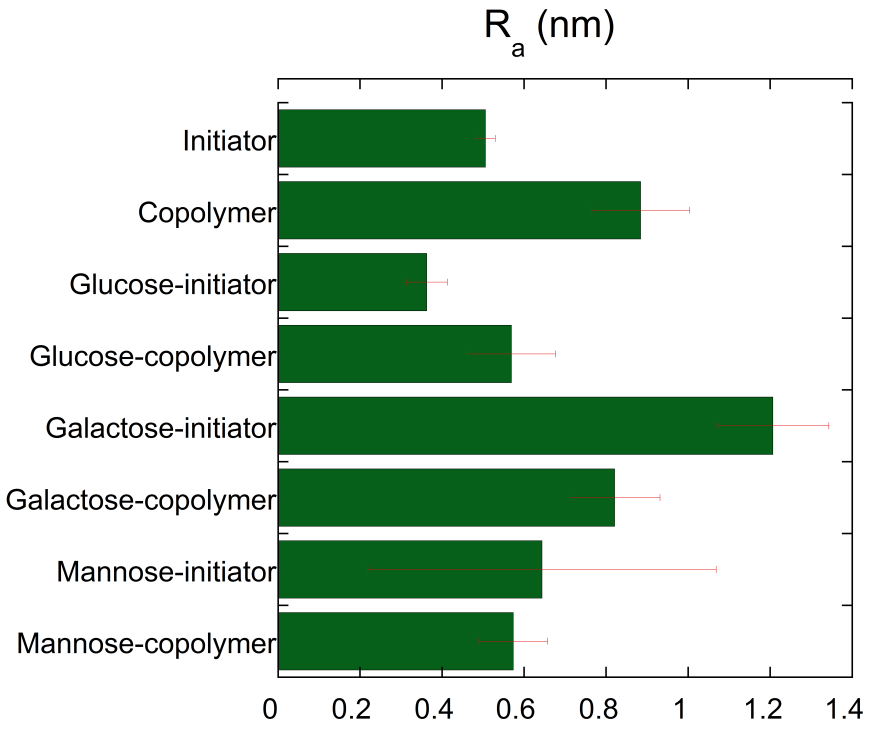

Figure S5. Surface roughness of coatings studies in this paper. The mean roughness (R_a) was used as a measure of surface roughness. All surfaces can be considered smooth since R_a values do not exceed 2 nm.

4 Adenovirus, fibrinogen, influenza on glucose & galactose polymer brushes

These figures are supplemental to Figure 2 in the main manuscript

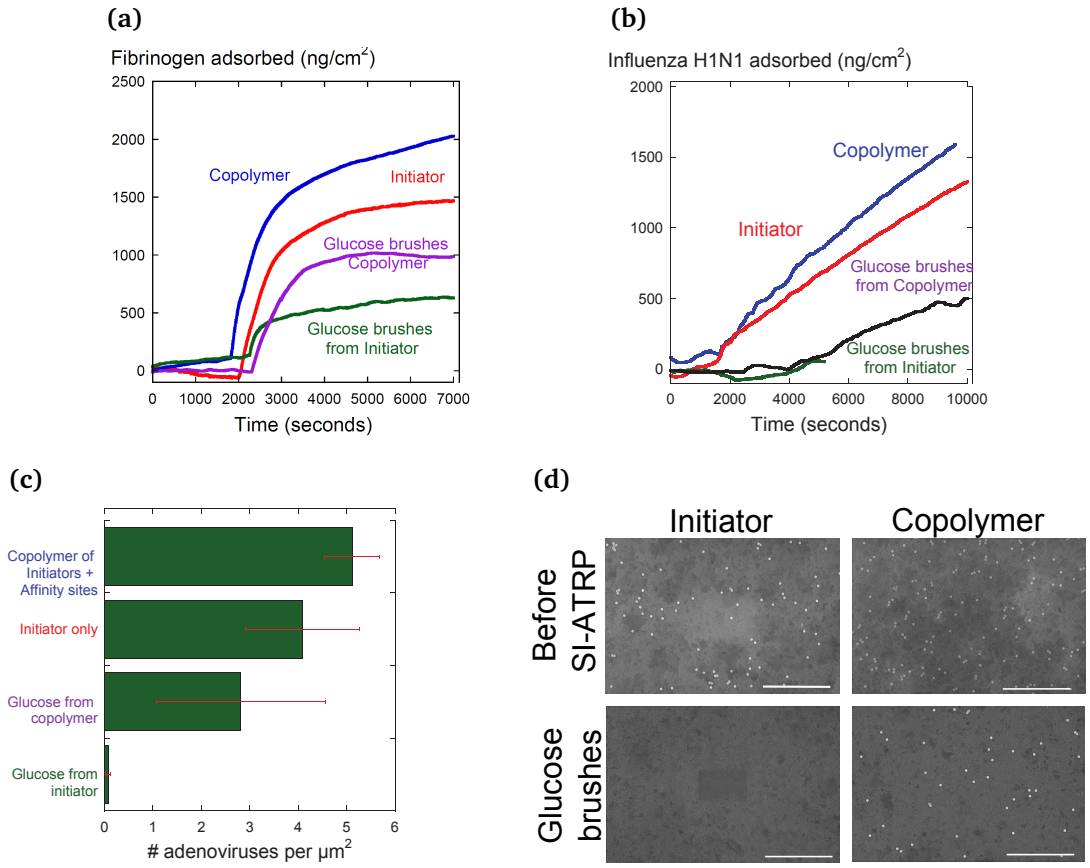

Figure S6. Adsorption kinetics of (a) fibrinogen and (b) Influenza H1N1 particles on surfaces to study the impact of AM binding sites and glucose brushes. In both (a) and (b), the presence of the aminomethyl promoted adsorption while the introduction of the glucose brushes had an inhibitory effect. (c) Quantification of adenovirus attachment on surfaces. (d) Representative SEM images. Scale bar: 5 μm. Adsorption trends mirrored those of fibrinogen and influenza.

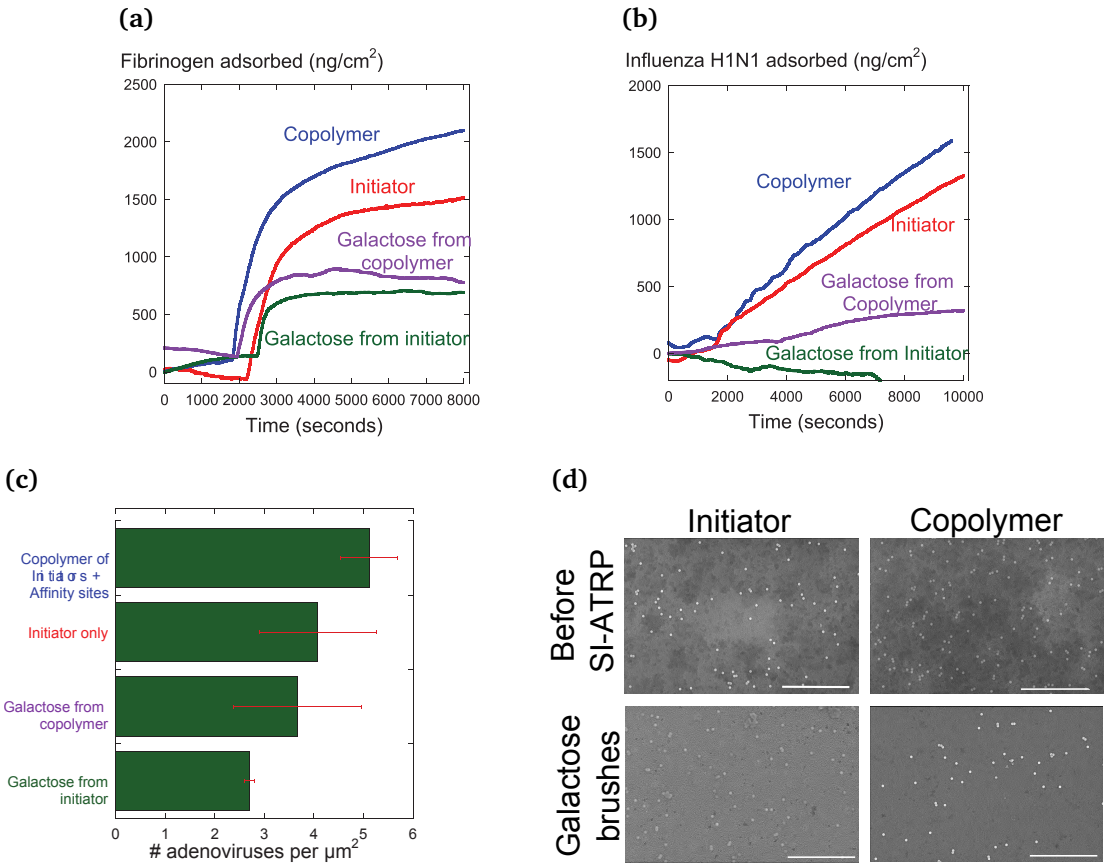

Figure S7. (a) Effect of surface composition on the adsorption kinetics of fibrinogen and (b) Influenza H1N1 particles on the surfaces studied. In both (a) and (b), the aminomethyl promoted adsorption while the galactose brushes suppressed it. (c) Quantification of adenovirus attachment on surfaces. (d) Representative SEM images. Scale bar: 5 μm. Adsorption trends were similar to the ones observed in fibrinogen and influenza.

5 Ellipsometric characterization

The kinetics of brush growth were assessed for glucose, galactose and mannose brushes grafted from reference polymer (PPX-EB) coatings. We observed a rapid increase in brush thickness in the time span between 0-4 hours and a subsequent plateauing of brush growth between 8-24 hours for all three carbohydrate brushes used.

Ellipsometric characterization was also performed for surfaces used in Figure 2 in the

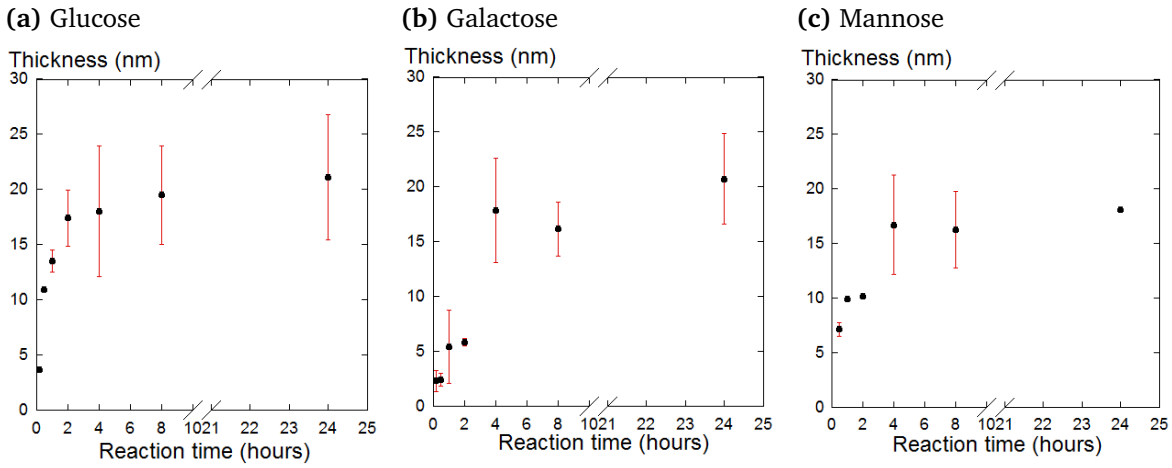

Figure S8. Evolution of brush thickness with time during SI-ATRP of
(a) poly(2'-acrylamidoethyl-β-d-glucopyranoside),
(b) poly(2'-acrylamidoethyl-β-d-galactopyranoside) and
(c)poly(2'-acrylamidoethyl-α-d-mannopyranoside)

main manuscript and for Figures S6 and S7 in SI. The initiator coatings (PPX-EB) and copolymer coatings used for glucose, galactose and mannose were synthesized in the same CVD polymerization and copolymerization run respectively to keep the composition consistent. SI-ATRP of PPX-EB and CP was performed in the same SI-ATRP run to maintain identical polymerization conditions. We could achieve higher brush thickness for carbohydrate polymers grafted from PPX-EB than from those grown on the copolymer coating. This trend was observed across all three brushes studied.

Table S1. Brush thickness for glucose, galactose and mannose brushes grafted from PPX-EB and the copolymer surfaces with a reaction time of 24 hours. Four substrates were used per sample group[1]

Coating	Thickness values (nm)				Mean (nm)	S.D (nm)
Glucose EB	20	12.1	17	16.7	16.5	3.3
Glucose CP	1.2	3.7	0	0	1.2	1.7
Galactose EB	5.8	10.1	3.6	5.9	6.4	2.7
Galactose CP	3.5	4	0	0	1.9	2.2
Mannose EB	16.9	17.9	–	–	17.4	0.7
Mannose CP	1.2	3	0	–	1.4	1.5

6 FTIR spectra

Following FTIR spectra were obtained for glucose, galactose and mannose brushes grafted from PPX-EB surfaces

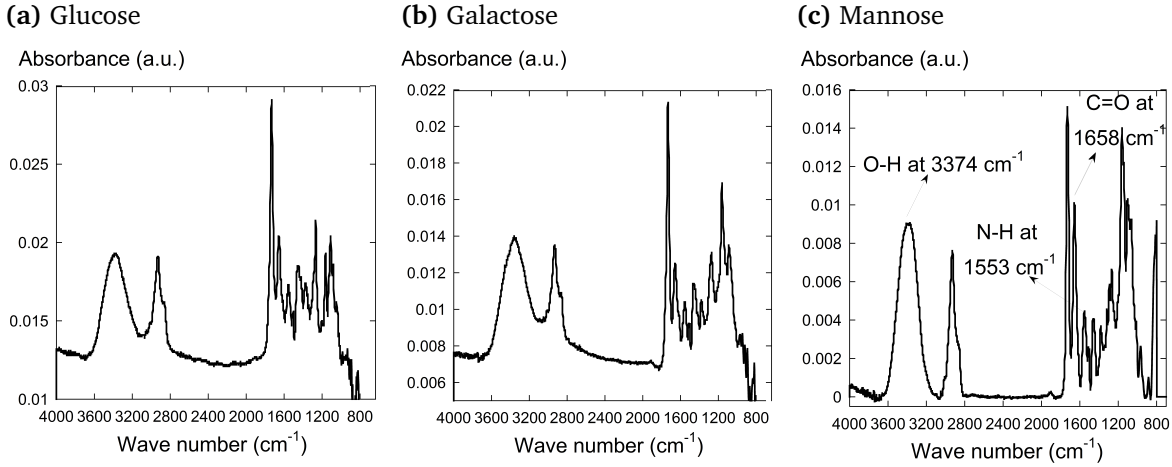

Figure S9. FTIR reference spectra for

(a) poly(2'-acrylamidoethyl-β-d-glucopyranoside),

(b) poly(2'-acrylamidoethyl-β-d-galactopyranoside)

(c)poly(2'-acrylamidoethyl-α-d-mannopyranoside)

[1]The symbol – indicates that no measurements were performed and a value of 0 indicates that no increase in coating thickness was detected upon SI-ATRP.

7 Contact angle measurements

Static contact angles of deionized water were measured using a contact angle goniometer (Ramé-Hart 200-F1 goniometer). Measurements were taken at three different locations and averaged for each substrate. Four substrates were used per sample group. In Figure S10, we estimated the increase in wettability caused by the incorporation of hydrophilic carbohydrate brushes on the hydrophobic parylene-based ATRP initiator coatings. A significant decrease in advancing contact angle was observed after grafting glucose, galactose and mannose brushes. We proceeded to compare the contact angles of the initiator coating, the copolymer coating and glucose brushes grafted from both these surfaces (Figure S11. While the initiator and copolymer exhibited comparable contact angles, it was interesting to observe that the glucose brushes grafted from the former were more hydrophilic than the ones grown on the latter. We attribute this to the reduced brush density and thickness on glucose brushes grafted from the copolymer, which results in wetting behaviour intermediate between those of the parylene coatings and the thick and dense carbohydrate brushes.

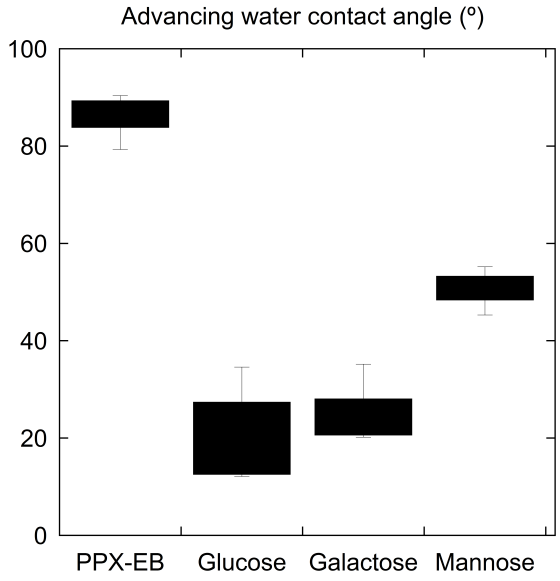

Figure S10. The contact angle values observed on the reference PPX-EB coatings were above 90 °, indicating a hydrophobic surface. After SI-ATRP of glucose, galactose and mannose brushes, the water contact angle reduced significantly, indicating that the grafting process had been successful, transforming a hydrophobic surface into a hydrophilic one.

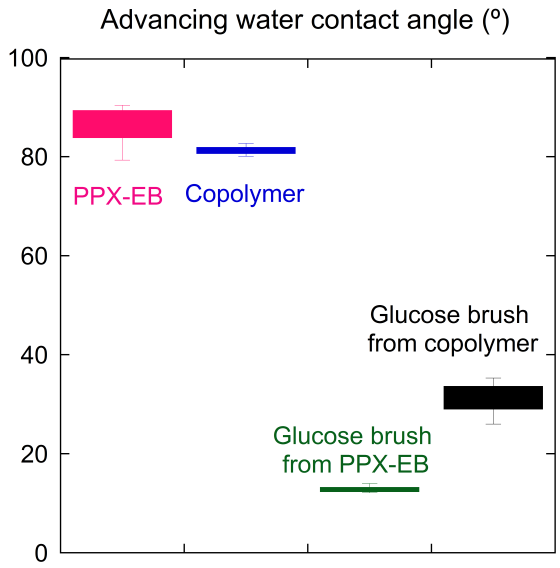

Figure S11. No significant differences were observed between contact angle values of the PPX-EB reference and copolymer surfaces. However, after SI-ATRP of glucose polymer, brushes grafted from the initiator was found to be more hydrophilic than those from the copolymer.

8 Characterization of influenza particles

Dynamic light light scattering revealed a size of 120 nm while electrophoretic mobility measurements indicated a ζ-potential of -28.5 mV

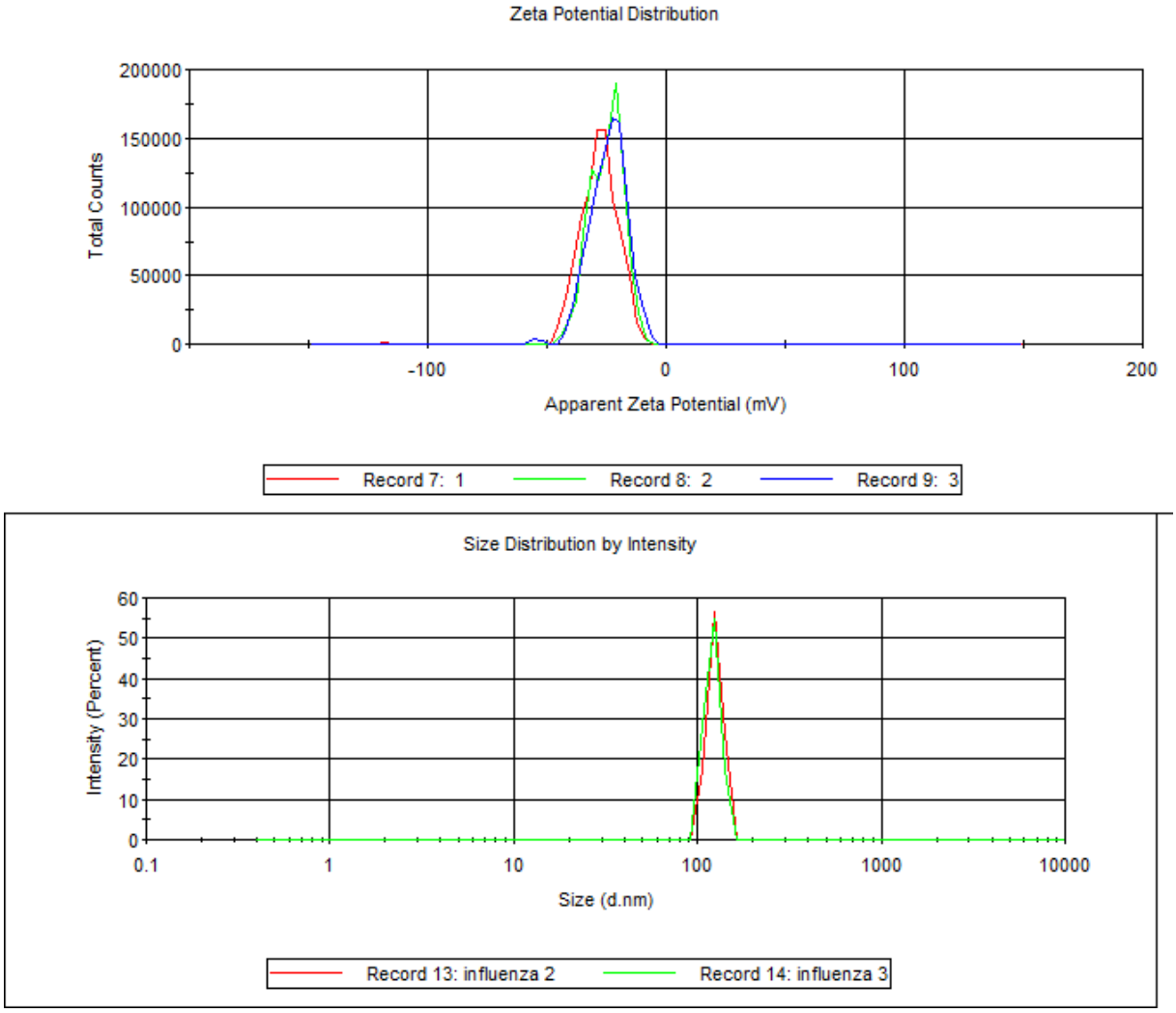

Figure S12. Hydrodyamic diameter and surface charge measurements of influenza A/PR/8/34 H1N1 particles.

9 Experimental

9.1 Synthesis of initiator and copolymer coatings.

The initiator coatings for SI-ATRP, poly[(*p*-xylylene-4-methyl-2-bromoisobutyrate)-*co*-(*p*-xylylene)] (PPX-EB)were prepared as described in Jiang et al.[3] Briefly, 32 mg of [2.2]paracyclophane-4-methyl 2-bromoisobutyrate (PCP-EB) was sublimed at 115-125 °C under reduced pressure (0.3 mbar) and then pyrolysed at 540 °C. The polymers were subsequently deposited on the substrates maintained at 14 °C.

Copolymer coatings comprised of [2.2]paracyclophane-4-methyl 2-bromoisobutyrate (PCP-EB) and 4-aminomethyl[2,2]paracyclophane (PCP-AM) were synthesized using a custom-built two-source CVD system.[4] In a typical experiment, 25 mg of PCP-AM and 80 mg of PCP-EB were loaded into the first and second tubes. Both source furnaces were heated to pyrolysis temperatures of 660 °C and 540 °C respectively using independently operated temperature controllers. In order to vary the ratio of the two functional groups deposited on the substrate, the separation distance between the precursor and the furnace was adjusted. For the PCP-EB precursor, this distance was maintained at 0.8 cm. For the copolymers CP44 through CP47, the separation between PCP-AM and the furnace was varied between 2.8 to 3.2 cm. For the copolymers CP40 through CP43, the separation between PCP-AM and the furnace was varied between 3 to 5 cm. Both precursors were sublimed between 80 °C and 110 °C at a pressure of 0.125 torr. The deposition chamber was cooled to 14 °C and the stage was rotated continuously to ensure uniform composition throughout the substrates. An argon flow rate of 10 standard cubic centimeters per minute was maintained in each tube and the sublimated dimers were transported into the pyrolysis zone by the argon carrier gas. Thereafter, they entered the deposition chamber to adsorb to the substrates and undergo copolymerization. Ultimately, coatings of poly[(*p*-xylylene-4-methyl-2-bromoisobutyrate)-*co*-(*p*-xylylene-4-aminomethyl)-*co*-(*p*-xylylene)] were formed on the substrates. Upon the complete sublimation of the PCP-EB precursor, deposition was

halted immediately.

9.2 Synthesis of monomers

In the first step, we synthesized 2'-acrylamidoethyl-2,3,4,6-tetra-O-acetyl-α-d-mannopyranoside, the monomer for SI-ATRP from α-d-mannose pentaacetate. For the first step, we broadly followed the synthetic procedure described by Wilkins et al.[5], with minor modifications. In the final step, we deprotected the latter to synthesize 2'-acrylamidoethyl-α-d-mannopyranoside. We opted for pre-polymerization deprotection instead of post-polymerization deprotection as the latter strategy is unlikely to yield quantitative conversion for surface-immobilized polymer brushes.

Briefly, 5 g (0.012moles) of α-d-mannose pentaacetate (Sigma Aldrich) was added to a clean and dry round-bottomed flask under argon. The solid was degassed using three cycles of vacuum-argon purging to remove adventitious moisture. Then, 50 mL of anhydrous dichloromethane was added under argon through a degassed needle and syringe. This mixture was stirred to dissolution under argon atmosphere and then cooled to 0-5 °C. Then, 2 mL (1.5 equivalents, 0.0188 moles) of hydroxy ethyl acrylamide (Sigma Aldrich) was injected into the reaction mass under argon. Finally 3.5 mL boron trifluoride diethyl etherate (1.2 equivalents, 0.015 moles) was added slowly over 15-30 minutes to the cooled reaction mass under argon. The flask was maintained at 0-5 °C for 30 minutes and then the reaction was allowed to proceed overnight at 22 °C. The next morning, the reaction mass was washed thoroughly with a saturated solution of sodium bicarbonate, then with deionized water and finally with a saturated solution of sodium chloride. The dichloromethane was removed at 37 °C in a rotavap until a yellow and oily crude was obtained. The crude was purified using column chromatography using a 7:3 mixture of ethyl acetate and n-hexane. The product was obtained by distilling off the ethyl acetate-hexane mixture under vacuum at 39 °C and 1.2 g of a white solid was obtained. After thorough drying on a schlenk line, this solid was analyzed using NMR to confirm the formation of

2'-acrylamidoethyl-2,3,4,6-tetra-O-acetyl-α-d-mannopyranoside.

In the second step, 40 mL of anhydrous methanol was added to 1 g (0.033 moles) of the above material and stirred to dissolution under argon. Then 2.3 mL of 25 % sodium methoxide in methanol (3 equivalents, 0.01 moles) was added slowly over 15 minutes under argon. The reaction mass was stirred for 1.5 hours under argon at 22 °C. Then a small quantity of the ion-exchange resin Dowex 500, which was pre-washed with methanol, was added to the reaction mass and stirred for 10 minutes. Then the Dowex was filtered off and the methanol filtrate was distilled at 37 °C in a rotavap to obtain a white foamy solid 2'-acrylamidoethyl-α-d-mannopyranoside. Similar procedures were adopted to synthesize 2'-acrylamidoethyl-β-d-galactopyranoside and 2'-acrylamidoethyl-β-d-glucopyranoside from their respective pentaacetate starting materials.

9.3 Surface-initiated atom transfer polymerization

Substrates bearing bromoisobutyryl groups (EB), either the homopolymer PPX-EB or the copolymer with PCP-AM, were prepared according to the CVD processes described above. The initial and final values of the coating thickness were ascertained using nulling ellipsometry before and after SI-ATRP. In a typical SI-ATRP run, copper (I) chloride, copper (II) chloride and Me_6Tren were purchased from Sigma Aldrich and used without further purification. Substrates were placed in a glove bag and degassed using 3 cycles of vacuum-argon purge and left at room temperature under argon. The respective carbohydrate-functionalized acrylamide monomer (2'-acrylamidoethyl-β-d-galactopyranoside or 2'-acrylamidoethyl-β-d-glucopyranoside or 2'-acrylamidoethyl-α-d-mannopyranoside) was synthesized as described previously. Typically, about 1 g of the monomer contained within a 50 mL flask was degassed using 3 cycles of vacuum-argon purges. In parallel, 25 mL of milli-Q water, 500 mg NaCl and 200 μL of Me_6Tren were added to a 50 mL schlenk flask and three cycles of freeze-pump thaw were performed. After completion of the third freeze operation, 29 mg CuCl and 3 mg $CuCl_2$ were added to the catalyst

flask under argon. Pump and thaw operations were continued subsequent to catalyst addition. Upon dissolution, the blue-colored catalyst mixture was transferred to the degassed monomer flask and mixed thoroughly at room temperature under argon atmosphere. This mixture was transferred to the glove bag and distributed such that each substrate was submerged completely in the reaction solution. The SI-ATRP reaction was allowed to proceed for either 1 hour or 24 hours under argon atmosphere. Finally, substrates were rinsed repeatedly with 0.05 M EDTA solution and deionized water and dried.

9.4 Ellipsometry

Ellipsometry was performed on silicon wafers (Silicon Valley Microelectronics, CA) assuming a native silicon dioxide layer of 2.5 nm thickness. Coating thickness was measured before and after SI-ATRP with a nulling ellipsometer (EP3 Nanofilm, Accurion GmbH, Germany). Ellipsometric delta and psi values were collected at a wavelength of 531.9 nm. Fixed values were used for the real (n=1.58) and imaginary (k=0) components of the refractive index of the polymer coatings. Using spectroscopic measurements, we verified that the refractive index of the initiator coating was very close to that of the carbohydrate brushes. After SI-ATRP, the thickness of the carbohydrate coatings formed was calculated by subtracting the initial thickness of the initiator layer from the post-ATRP thickness. Two substrates were used per experimental run.

9.5 Fourier transformed infrared spectroscopy

To verify whether the desired functional groups were present on the surface of the polymer coatings, Fourier-transformed infrared (FTIR) spectroscopy was performed using Nicolet 6700 spectrophotometer in the grazing angle configuration against a gold background. Polymers were deposited on gold wafers and 128 scans were collected with a resolution of 4 cm^{-1}. The absorbance intensities were normalized using the OMINIC software.

9.6 X-ray photoelectron spectroscopy

XPS was performed on an Axis Ultra X-ray photoelectron spectrometer (Kratos Analyticals, UK) equipped with a monochromatized Al-Kα X-ray source. All peaks were calibrated with respect to the non-functionalized aliphatic carbon with a binding energy of 285.0 eV. The area under each high resolution spectra was quantified and elemental compositions calculated using relative sensitivity factors of 1, 2.93, 2.84 and 1.8 for C_{1s}, O_{1s}, Br_{3d} and N_{1s} respectively. Peak fitting and analysis was performed using Casa XPS software.

9.7 Modeling

For the statistical models, the Poisson cumulative distribution functions were calculated as a function of actual amine density on the copolymer surface and the critical amine density required for viral capture. The latter is dependent on the dissociation constant (K_{eq}) of aminomethyl, which is assumed to be of 10^5 and the pH value. The area of the electrostatic zone of influence was determined as per the Derjaguin approximation. The interaction energy was calculated as the sum of the three terms, U_{VDW}, U_{EDL} and U_{brush}. For the Van Der Waals contribution to the interaction energy, we assumed a Hamaker constant of 10^{-20} J and a particle radius of 20 nm. U_{EDL}, stemming from electrostatic interactions, was quantified by assuming a virus surface charge of -43.5 mV and a Debye Length of 1 nm. For surfaces from which brushes were grafted, U_{brush}, the interaction energy was first calculated assuming a Kuhn length of 0.2 nm, excluded volume of 0.5 nm^3 and a grafting density of 0.4 chains/nm^2. Both elastic energy and excluded volume contributions were considered in calculating U_{brush}.

9.8 Quartz crystal microbalance measurements

The QCM-200 instrument (Stanford Research Systems, CA) was used for these studies. AT-cut quartz crystals coated with chrome/gold (O100RX1, Stanford Research Systems, CA) were functionalized with polymer coatings as described in earlier sections.

For fibrinogen measurements, the following procedure was employed. Prior to measurement, the polymer-coated crystal surfaces were allowed to equilibrate overnight in a solution of 10 mM phosphate buffered saline (PBS). After the crystal was mounted on a flow cell, a syringe pump was employed to circulate the PBS through the flow cell at a rate of 0.1 mL/hour. Once a stable baseline was established, the pump inlet was switched from PBS to a reservoir containing the fibrinogen solution in PBS (concentration of 10 μg/mL). This solution was injected into the flow cell for over 5000 seconds and the adsorption response recorded at intervals of 1 second. The adsorbed fibrinogen mass was computed from the frequency decrease through the Sauerbrey equation.

For influenza H1N1 adsorption measurements, a similar procedure was employed. Influenza A/PR/8/34 H1N1 strain was obtained from Charles River avian vaccine services (catalog # 10100782). Again, the polymer-coated crystal surfaces were allowed to equilibrate overnight in a solution of 10 mM PBS. Then, the crystal was mounted on a flow cell and the PBS buffer was pumped through the flow cell at a flow rate of 0.1 mL/hour using a syringe pump. Once a stable baseline was observed, the pump inlet was switched over to a reservoir of the influenza suspension in PBS (diluted to achieve a final concentration of 500 HA units/mL). This suspension was injected into the flow cell for over 5000 seconds and the adsorption response recorded at intervals of 1 second. The adsorbed mass of the virus was computed from the frequency decrease through the Sauerbrey equation.

9.9 Adenovirus adsorption measurements

Silicon wafers (0.5 cm $\times$ 0.5 cm in size) were functionalized with the desired polymer coatings as described earlier. These wafers were placed in a 24-well plate and sterilized with 70% ethanol for 30 minutes. Thereafter, they were washed 5 $\times$ 5 minutes with sterile PBS. Then, 1 mL of a solution of Ad-pLpA (obtained from the University of Michigan's Vector Core) was added to each of the wells and incubated for 3-4 hours at 4 $^{\circ}$C while being shaken gently. The viral concentration was maintained at 1 $\times$ 10^{11} particles/mL. The virus

solution was subsequently aspirated and the wafers washed 5 $\times$ 5 minutes with sterile PBS. Finally the viruses adsorbed to the polymer coatings were fixed using 2.5 % paraformaldehyde (Electron Microscopy Services) in PBS. The samples were then dehydrated in ethanol and dried in a dessicator overnight. Viral adsorption was compared across different surfaces using scanning electron microscopy. Samples were mounted on a copper-taped SEM stub and sputter-coated with gold for 120 seconds. All images were acquired at 10,000 $\times$ magnification using the FEI Helios 650 nanolab instrument. For each sample group, viral particles were counted manually twice from four images for each sample group. Bright particles of the size range 50-100 nm were included in the count.

References

(1) Duffadar, R.; Kalasin, S.; Davis, J. M.; Santore, M. M. *Journal of Colloid and Interface Science* **2009**, *337*, 396–407.

(2) Bendersky, M.; Santore, M. M.; Davis, J. M. *Journal of Colloid and Interface Science* **2015**, *449*, 443–451.

(3) Jiang, X.; Chen, H.-Y.; Galvan, G.; Yoshida, M.; Lahann, J. *Advanced Functional Materials* **2008**, *18*, 27–35.

(4) Elkasabi, B. Y.; Chen, H.-y.; Lahann, J. *Advanced Materials* **2006**, *18*, 1521–1526.

(5) Wilkins, L. E.; Phillips, D. J.; Deller, R. C.; Davies, G.-L.; Gibson, M. I. *Carbohydrate Research* **2015**, *405*, 47 – 54, Glyconanomaterials.